

Optimization of Condition of Ultrasonic Beam for Measurement of Small Change in Thickness of Arterial Wall

Masaru WATANABE*, Hideyuki HASEGAWA† and Hiroshi KANAI‡

Department of Electrical Engineering, Tohoku University Graduate School of Engineering, Aramaki-aza-Aoba 05, Aoba-ku, Sendai 980-8579, Japan

(Received November 20, 2001; accepted for publication January 22, 2002)

We previously developed a method for measuring small changes in thickness of the arterial wall during one cardiac cycle. Knowledge of this change in thickness is useful for *in vivo* assessment of the regional elasticity of the arterial wall. In this study, from computer simulations, it is found that measurement error depends on the distance of the ultrasonic beam from the center of the artery and it can be reduced by optimally setting the focal position. In basic experiments using a silicone rubber tube and in *in vivo* experiments with a human carotid artery, it is found that by optimizing the focal position, measurement of the change in thickness becomes more robust against mispositioning of the ultrasonic beam. From these results, it is demonstrated that optimum focal positioning provides more robustness in measurement, even if there is arterial wall motion causing the position of the ultrasonic beam to deviate from the center of the artery. [DOI: 10.1143/JJAP.41.3613]

KEYWORDS: atherosclerosis, change in thickness of arterial wall, computer simulation, acoustic lens, focus

1. Introduction

The increase in the number of individuals suffering from acute myocardial or cerebral infarction, both of which are mainly caused by atherosclerosis, has become a serious clinical problem. It is, therefore, important to diagnose atherosclerosis at an early stage. However, to date, there are no methods available for the detection of minute changes in the elasticity of the arterial walls due to early-stage atherosclerosis.

We have developed a method for evaluating the elasticity within about $400\ \mu\text{m}$ of each local region in the arterial wall¹⁾ to diagnose vulnerability of atherosclerotic plaques. In our method, the small change in thickness of the arterial wall due to the heartbeat is accurately measured in each local region around the focal area of the ultrasonic beam. From the resultant change in thickness, the regional strain and the elasticity of the arterial wall are noninvasively evaluated.²⁾ By scanning the ultrasonic beam, the spatial distribution of the elasticity is also obtained.

In this measurement, however, accuracy is influenced by the setting of the electric focal depth. In our previous paper, the optimum ultrasonic focal position of electric focusing of the linear array probe was investigated for accurate measurement of the change in thickness.³⁾ Another effective method for reducing this influence is setting multiple focal points along one scan line, as is done in commercial ultrasonic diagnostic equipment. In multiple focusing, however, the time interval between successive scans for the same focal points increases. In our measurement of the change in thickness of the arterial wall, the time interval between successive scans must be less than 5 ms to prevent aliasing due to the assumption that maximum velocity of the arterial wall is 5 mm/s. In this study, therefore, *in vivo* measurement of small changes in thickness is simulated for single focusing in order to prevent aliasing.

In addition to the electric focal position, another factor which decreases the accuracy in measurement is mispositioning of the ultrasonic beam. Mispositioning means that the ul-

trasonic beam does not pass through the exact center of the artery, which occurs when the sonographer does not correctly maintain the position of the ultrasonic probe and/or movement of the arterial wall causes the position of the ultrasonic beam to deviate from the center of the artery. In this study, ultrasonic propagation in 3-D space is simulated in order to investigate the optimum ultrasonic focal position of the acoustic lens of the linear array probe in order to reduce the influence of the deviation of the position of the ultrasonic beam from the center of the artery. From basic experiments and *in vivo* experiments, by optimizing the focal position, it is demonstrated that the change in thickness can be measured accurately even if the position of the ultrasonic beam slightly deviates from the center of the artery.

2. Principle of Computer Simulation for Measurement of Small Change in Thickness

In the simulation, an arbitrarily shaped reflector in the $x - y - z$ space, which corresponds to a tube, is divided into many small scatterers as shown in Fig. 1. An electric scanning linear probe with $(2N + 1)$ elements is employed. The distance from

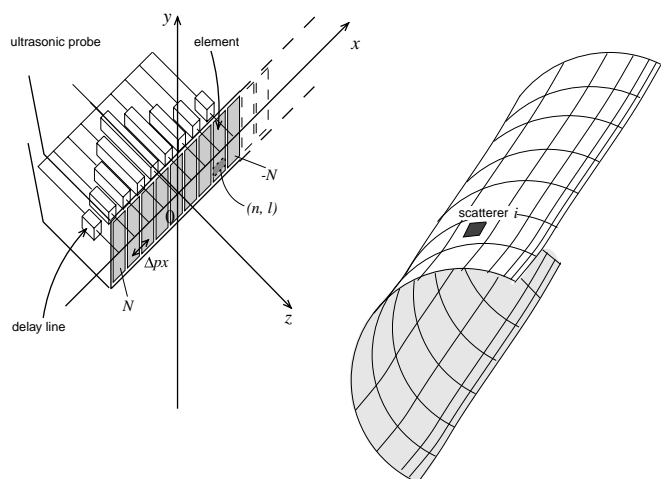


Fig. 1. Geometry of simulation model.

*E-mail address: watanabe@us.ecei.tohoku.ac.jp

†E-mail address: hasegawa@us.ecei.tohoku.ac.jp

‡E-mail address: hkanai@ecei.tohoku.ac.jp

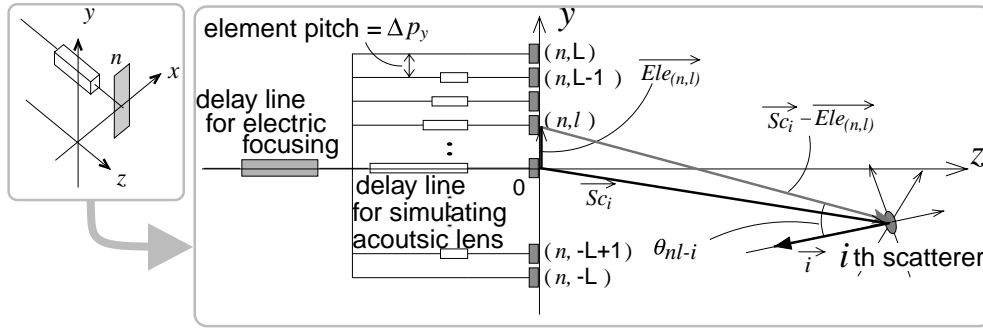


Fig. 2. Simulation of acoustic lens.

the n th element ($-N \leq n \leq N$) to the electric focal point at a depth of $z = d_f$ is given by $\sqrt{d_f^2 + (n \cdot \Delta p_x)^2}$, where Δp_x denotes the element pitch along the x -axis. In addition, to simulate characteristics of the acoustic lens, each element is divided into $(2L + 1)$ point-sources along the y -axis and the distance between the point-source is Δp_y , as shown in Fig. 2. Thus, in order to focus the ultrasonic pulses transmitted from $(2N + 1)$ elements, where each element consists of $(2L + 1)$ point sources, on each focal point (electric focal point: $z = d_f$, acoustic focal point: $z = d_{fac}$), the following delay time τ_{nl} is added to the delay line connected to the l th point-source in the n th element:

$$\tau_{nl} = \frac{\sqrt{d_f^2 + (N \cdot \Delta p_x)^2} - \sqrt{d_f^2 + (n \cdot \Delta p_x)^2}}{c} + \frac{\sqrt{d_{fac}^2 + (L \cdot \Delta p_y)^2} - \sqrt{d_{fac}^2 + (l \cdot \Delta p_y)^2}}{c}, \quad (-N \leq n \leq N, \quad -L \leq l \leq L) \quad (1)$$

where c is the sound speed. The first term on the right-hand side simulates the electric focal system along the x -axis, and the second term simulates the acoustic lens characteristics along the y -axis.

The incident angle, θ_{nl-i} , from the (n, l) th element of the probe to the i th small scatterer on the surface of the reflector is determined by the regional shape of the reflector and the geometrical relationship between the (n, l) th element and the scatterer. The incident angle, θ_{nl-i} , is described by the position vector, $\vec{Ele}_{(n,l)}$, of the (n, l) th transmitting element of the probe, the position vector, \vec{S}_{c_i} , of the i th scatterer, and the normal vector, \vec{i} , of the surface of the reflector at the position of the i th small scatterer as follows:

$$\cos \theta_{nl-i} = \frac{(\vec{S}_{c_i} - \vec{Ele}_{(n,l)}) \cdot \vec{i}}{|\vec{S}_{c_i} - \vec{Ele}_{(n,l)}| |\vec{i}|}. \quad (2)$$

By assuming a mirror reflection, the ultrasonic pulse is reflected with the same angle θ_{nl-i} . The receiving angle, $\varphi_{i-n'l'}$, from the i th scatterer to the receiving (n', l') th element is determined in the same manner, as follows:

$$\cos \varphi_{i-n'l'} = \frac{(\vec{0}, \vec{0}, \vec{1}) \cdot (\vec{Ele}_{(n',l')} - \vec{S}_{c_i})}{|(\vec{0}, \vec{0}, \vec{1})| |\vec{Ele}_{(n',l')} - \vec{S}_{c_i}|}. \quad (3)$$

The amplitudes of the incident wave and the received wave

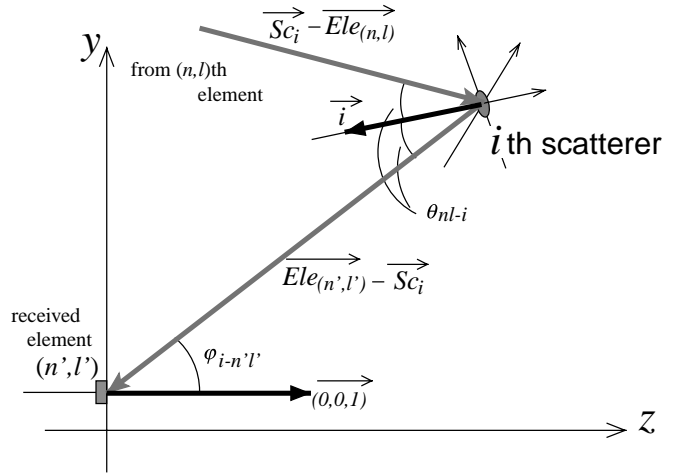


Fig. 3. Receiving angle, $\varphi_{i-n'l'}$.

depend on these values of $\cos \theta_{nl-i}$ and $\cos \varphi_{i-n'l'}$, respectively.

Each traveling time, τ'_{nl-i} , from the (n, l) th element to the i th small scatterer, and $\tau''_{i-n'l'}$, from the i th small scatterer to the (n', l') th element is determined by dividing the distance by sound velocity, c , as follows:

$$\tau'_{nl-i} = \frac{|\vec{Ele}_{(n,l)} - \vec{S}_{c_i}|}{c}, \quad (4)$$

$$\tau''_{i-n'l'} = \frac{|\vec{S}_{c_i} - \vec{Ele}_{(n',l')}|}{c}. \quad (5)$$

The RF ultrasonic wave $y_{n'l'}(t)$ received at the (n', l') th element is given by the summation of the reflective waves at all scatterers $\{i\}$ for the transmitted signal with an angular frequency $\omega_0 = 2\pi f_0$ radiated from all elements $\{(n, l)\}$ as follows:^{4,5)}

$$y_{n'l'}(t) = \sum_{n=-N}^N \sum_{l=-L}^L W(t - \tau_{nl}) \cdot \sin \omega_0(t - \tau_{nl}) * \left(\sum_i \delta(t - \tau'_{nl-i}) \cdot \cos \theta_{nl-i} * \delta(t - \tau''_{i-n'l'}) \cdot \cos \varphi_{i-n'l'} \right), \quad (6)$$

where $W(t)$ is the Hanning window employed to describe the transmitted pulse waveform, $*$ is the convolution operation,

and $\delta(t)$ is Dirac's delta function. The output RF signal $y(t)$ of the probe is given by the delayed summation of the RF ultrasonic wave received at all elements $\{(n, l)\}$ as follows:

$$y(t) = \sum_{n'=-N}^N \sum_{l'=-L}^L y_{n'l'}(t) * \delta(t - \tau_{n'l'}). \quad (7)$$

By applying quadrature demodulation to the output signal, $y(t)$, the change in thickness, $\Delta\hat{h}(t)$, is estimated by the *phased tracking method*.⁶⁾

3. Experiments by Computer Simulation

3.1 Simulated object

The simulated object is a tube with an inner radius of 3.4 mm, an outer radius of 4 mm, and a length of 20 mm. The object is divided into 28,800 scatterers with a circumferential pitch of 2 degrees and a longitudinal pitch of 250 μm . Let us assume that the inner surface and the outer surface have velocity signals, $v_i(t)$ and $v_o(t)$, in the direction away from the center of the tube as follows:

$$v_o(t) = \alpha \Delta d_{\text{max}} \cdot 2\pi f_{\text{rot}} \sin(2\pi f_{\text{rot}} t), \quad (8)$$

$$v_i(t) = (\alpha + 1) \Delta d_{\text{max}} \cdot 2\pi f_{\text{rot}} \sin(2\pi f_{\text{rot}} t), \quad (9)$$

where α is a constant that determines the difference between $v_i(t)$ and $v_o(t)$. The actual change in thickness $\Delta h(t)$ is obtained by integrating the difference between $v_o(t)$ and $v_i(t)$ as follows:

$$\Delta h(t) = \int_0^t \{v_o(t) - v_i(t)\} dt. \quad (10)$$

In the following experiments, the parameters are set as follows: $\alpha = 0.5$, $f_{\text{rot}} = 1.5$ Hz, $f_0 = 7.5$ MHz, $c = 1,480$ m/s, and the pulse repetition frequency (PRF) = 1 kHz.

During one cardiac cycle T , the RMS error, e_{rms} , of the estimated change in thickness, $\Delta\hat{h}(t)$, from the actual change in thickness, $\Delta h(t)$, is defined as follows:

$$e_{\text{rms}} = \sqrt{\frac{1}{T} \int_0^T \{\Delta h(t) - \Delta\hat{h}(t)\}^2 dt}. \quad (11)$$

3.2 Investigation of bias error caused by mispositioning of the ultrasonic beam

Figure 5(a) shows the M-mode image for the posterior wall of the tube obtained at a distance, d_l , of 1 mm from the *center axis* of the tube to the ultrasonic beam as shown in Fig. 4. The time interval, T , between the transmission timing pulse train in Fig. 5(b) shows one cycle of the change in thickness. By tracking the two points set in the posterior wall at the peak of the timing pulse, velocity signals, $v_i(t)$ and $v_o(t)$, are estimated by the *phased tracking method*,⁶⁾ as shown in Figs. 5(c) and 5(d). The change in thickness, $\Delta\hat{h}(t)$, is estimated by integrating the difference between these velocity signals, as shown in Fig. 5(e). The actual change in thickness, $\Delta h(t)$, of Eq. (10) is superimposed on the estimated one in Fig. 5(e). Figure 6 shows the estimation error, e_{rms} , plotted as a function of the distance, d_l , from the beam position to the *center axis* of the tube for five different settings of the focal depth, d_{fac} , of the acoustic lens. In these experiments, the electrical focal depth, d_f , is set precisely at the upper surface of the posterior wall of the tube. At the same d_l , the estimation error, e_{rms} , changes with the focal depth, d_{fac} , and is determined

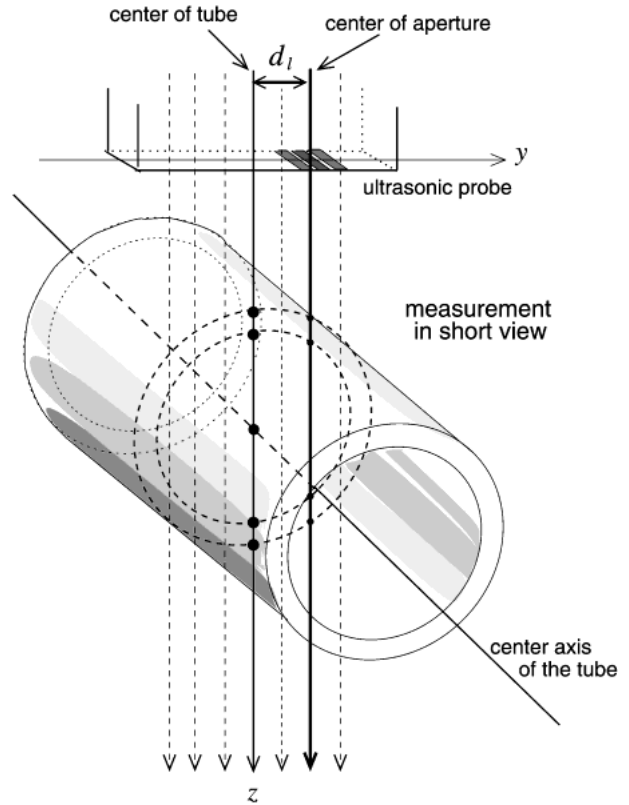


Fig. 4. Definition of the distance, d_l , from the ultrasonic beam to the center of the tube/artery.

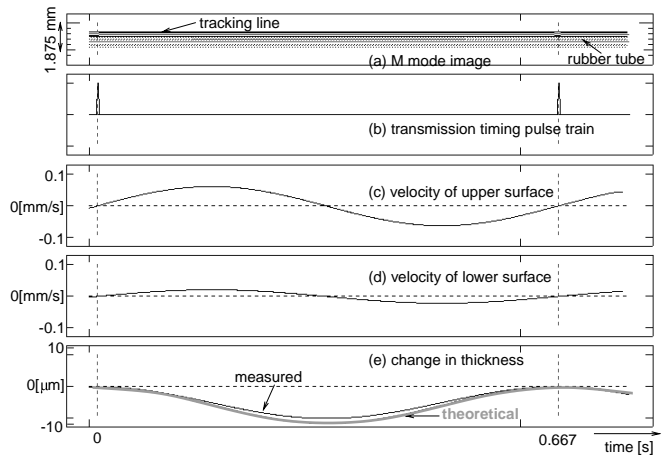


Fig. 5. Result of estimation of the change in thickness. (a) M-mode image; (b) the transmission timing pulse train; (c) (d) velocity signals, $v_i(t)$ and $v_o(t)$, of the tube surface; (e) the measured and theoretical changes in thickness, $\Delta\hat{h}(t)$ and $\Delta h(t)$.

by the characteristics of the acoustic lens in the case of longitudinal measurement. When d_l is shorter than 0.4 mm, high accuracy is achieved with every setting of the focal depth, d_{fac} . When d_l is greater than 0.4 mm, estimation error, e_{rms} , is suppressed by setting the focal depth, d_{fac} , farther from the object (d_{fac} is set at 27 mm and 34 mm). For the focal depth setting of 41 mm, however, measurement error cannot be suppressed. From these results, it is found that measurement error depends upon the position, d_l , of the ultrasonic beam and that it is reduced by setting the focal position, d_{fac} , of the acoustic lens farther from the object. As a result, accurately measur-

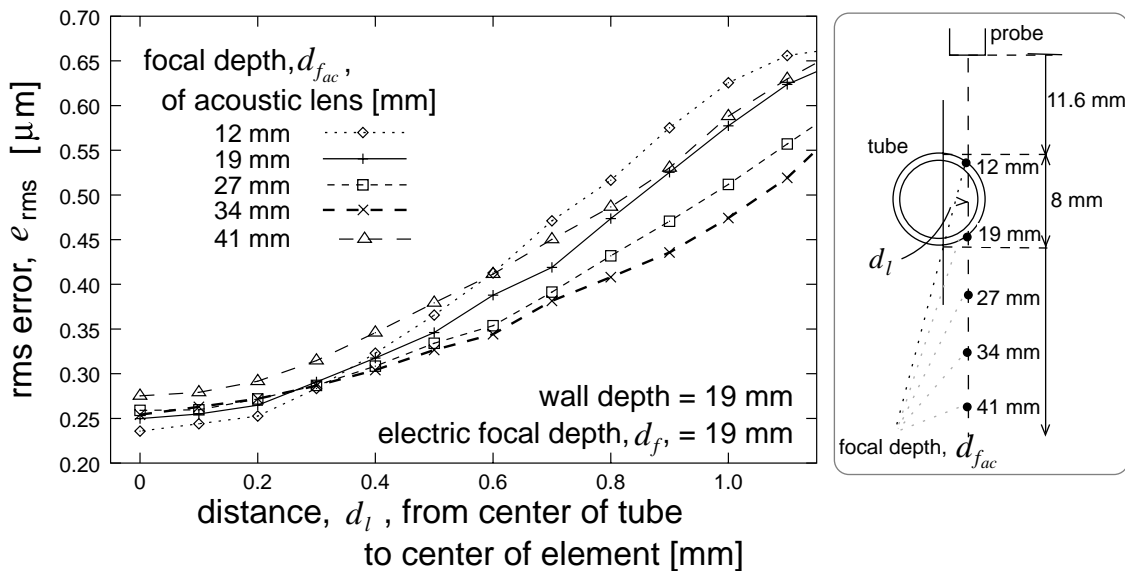


Fig. 6. Result of computer simulation for each characteristic of the acoustic lens.

able area of d_l is extended by optimizing the focal depth, d_{fac} , of the acoustic lens.

4. Results of Basic Experiments Using a Silicone Rubber Tube

Measurement accuracy has been evaluated for various values of the focal position, d_f , in experiments using a silicone rubber tube, in which the pulsatile flow is induced by an artificial heart.⁷⁾ The change in thickness, $\Delta\hat{h}(t)$, of the tube wall is generated by the pressure change caused by the arrival of the pulsatile flow.

Figure 7(a) shows the M-mode image of the tube obtained for the case where the distance, d_l , from the ultrasonic beam to the center axis of the tube is 0.3 mm. Figure 7(b) shows the driving pulse of the artificial heart. Figure 7(c) shows the inner pressure upstream of the ultrasonic measurement position. By tracking the two points set in the posterior wall when the driving signal rises, velocity signals, $v_i(t)$ and $v_o(t)$, are estimated by the *phased tracking method*, as shown in Figs. 7(d) and 7(e). Figure 7(f) shows the change in thickness, $\Delta\hat{h}(t)$, which is obtained by integrating the difference between these velocity signals. The maximum amplitude, Δh_{max} , of the change in thickness, $\Delta\hat{h}(t)$, is about $4\ \mu\text{m}$ for every three heart beats. The elastic modulus of the silicone rubber tube employed in basic experiments is 2.4 MPa.²⁾ The actual maximum amplitude of the change in thickness of the tube is obtained as $4.1\ \mu\text{m}$ from the elastic modulus, the thickness of the wall, the inner radius of the tube and the change in inner pressure.

In Fig. 8, the maximum amplitude of the change in thickness is plotted as a function of distance, d_l , from the beam position to the center of the tube for four different settings of the electric focal depth, d_f . When the electric focal depth, d_f , is set at 19 mm, which is the same depth as that of the inner surface of the posterior wall, the change in thickness, $\Delta h(t)$, can be measured with high accuracy only around the center axis of the tube. The measurement accuracy decreases significantly when distance, d_l , from the ultrasonic beam to the

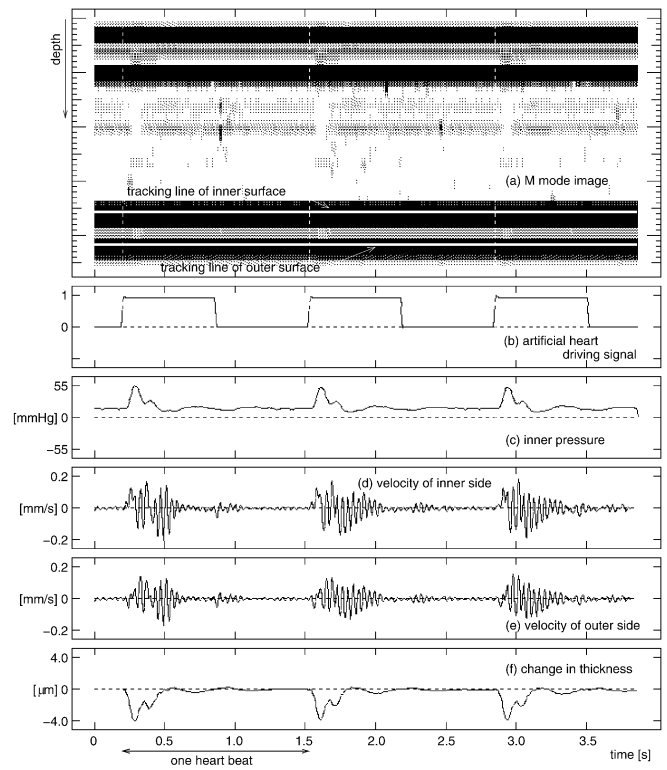


Fig. 7. Results of measurement of the change in thickness of the tube wall obtained at the center of the tube. (a) M-mode image; (b) artificial heart driving signal; (c) inner pressure; (d) (e) velocity signals, $v_i(t)$ and $v_o(t)$, of both surfaces of the tube; (f) estimated change in thickness, $\Delta\hat{h}(t)$.

center of the tube is greater than 0.5 mm. On the other hand, when the electric focal depth, d_f , is set deeper than that of the outer surface of the posterior wall, high accuracy is achieved in a broader region up to 1.5 mm from the center axis.

Using a broadened ultrasonic beam, the change in thickness is accurately estimated from the ultrasonic wave reflected from the region around the center axis on the posterior wall even when the beam position, d_l , is farther from the center axis. It is found that the measurement error dependent upon the position, d_l , of the ultrasonic beam is reduced by

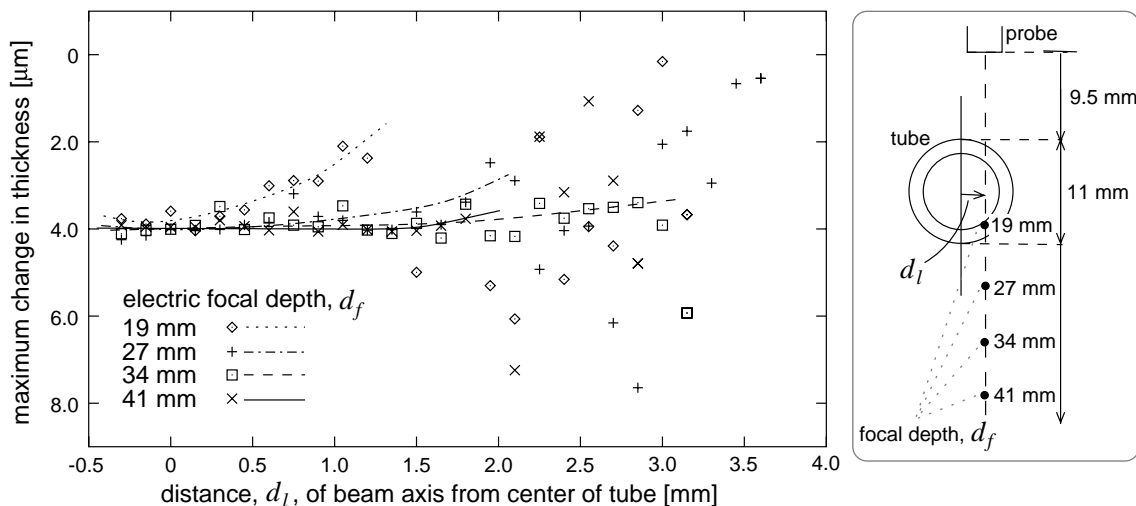


Fig. 8. The maximum change in thickness is plotted as a function of distance of the beam from the center of the tube.

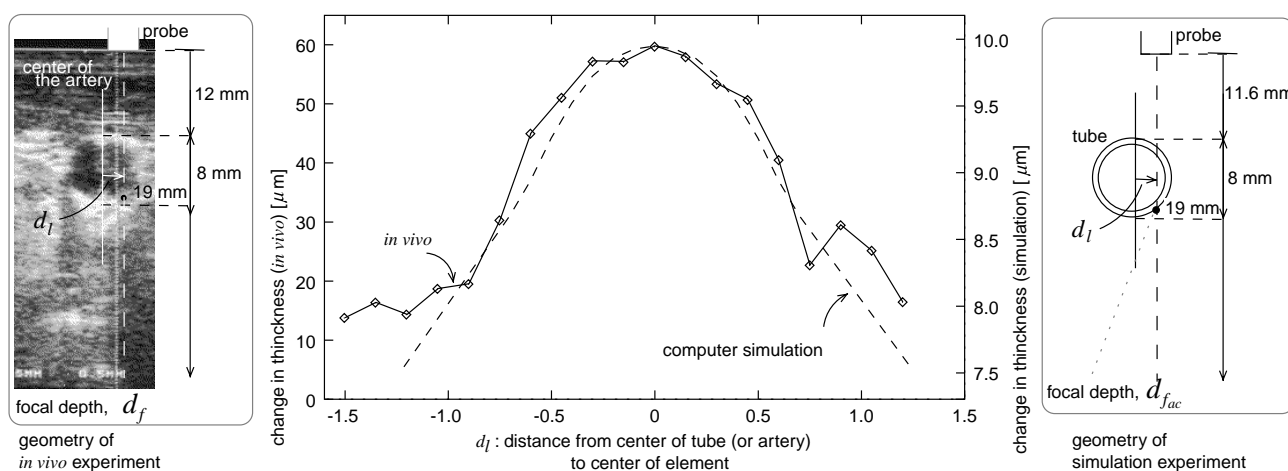


Fig. 9. Comparison between results of *in vivo* measurement and computer simulation.

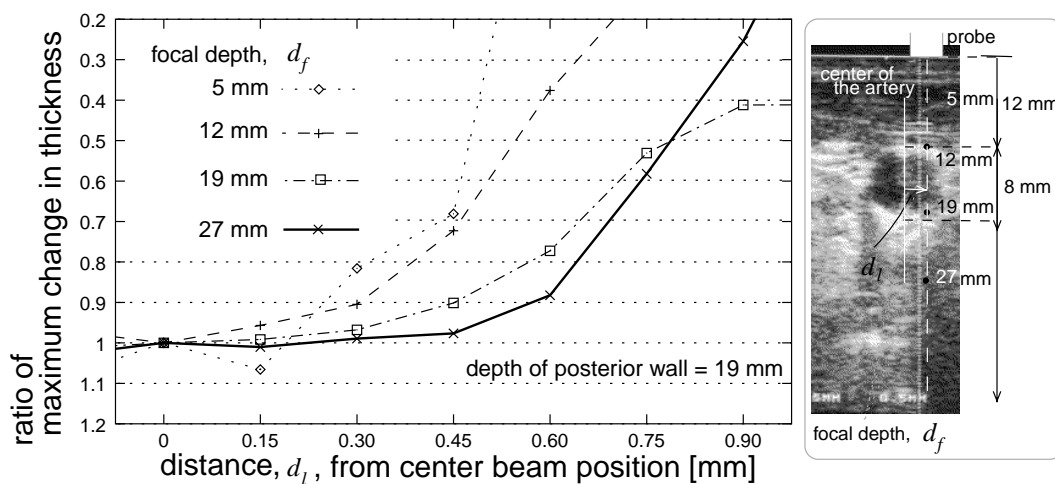


Fig. 10. Results of *in vivo* measurement for each setting of focal position.

setting the focal position, d_f , farther from the object, which is also estimated in the simulation experiments.

5. *In vivo* Experimental Results

Measurement accuracy is evaluated in *in vivo* measurement at the human common carotid artery under the condition of an electric focal depth, d_f , of 19 mm.⁸⁾

Figure 9 shows the maximum amplitude, $\Delta\hat{h}_{\max}$, of the change in thickness obtained as a function of the distance, d_l , of the ultrasonic beam from the *center axis* of the artery. The maximum amplitude, Δh_{\max} , of the change in thickness obtained by computer simulation is also plotted in Fig. 9. From Fig. 9, it is found that *in vivo* experimental results are well described by computer simulation. Figure 10 shows the ratio of the maximum amplitude, $\Delta\hat{h}_{\max}$, of the change in thickness measured at each beam position to that measured at the *center axis*. It is plotted for other settings of the focal depth of 5 mm, 12 mm and 27 mm. From Fig. 10, it is also shown by *in vivo* measurement that the change in thickness can be accurately measured in a broader region by setting the focal position farther from the object.

6. Conclusions

In this study, ultrasonic propagation in 3-D space is simulated to investigate the optimum focal position, which makes measurement of the change in thickness more robust against lateral change, d_l , in the position of the ultrasonic beam. From

basic and *in vivo* experiments, it is confirmed that the region where the change in thickness, $\Delta h(t)$, is accurately measured is extended to ± 0.45 mm around the center of the artery by setting the electric focal position, d_f , deeper than the posterior wall of the artery. This result provides successful *in vivo* measurement of the change in thickness, which is less sensitive to the position, d_l , of the ultrasonic beam.

- 1) H. Kanai, H. Hasegawa, N. Chubachi, Y. Koiwa and M. Tanaka: IEEE Trans. UFFC **44** (1997) 752.
- 2) H. Hasegawa, H. Kanai, N. Hoshimiya and Y. Koiwa: Proc. IEEE Ultrasonics Symp. (2000) 1829.
- 3) M. Watanabe and H. Kanai: Jpn. J. Appl. Phys. **40** (2001) 3918.
- 4) J. H. Lee and S. W. Choi: IEEE Trans. UFFC **47** (2000) 644.
- 5) S. K. Jespersen, P. C. Pedersen and J. E. Wilhjelm: IEEE Trans. UFFC **45** (1998) 1461.
- 6) H. Kanai, M. Sato, Y. Koiwa and N. Chubachi: IEEE Trans. UFFC **43** (1996) 791.
- 7) M. Takano, H. Kanai, N. Chubachi, Y. Koiwa, F. Tezuka and M. Takahashi: J. Acoust. Soc. Jpn. **51** (1995) 174 [in Japanese].
- 8) M. Watanabe, H. Hasegawa and H. Kanai: Ultrason. Electron. Meet. Tohoku Univ. **30-4** (2001) [in Japanese].